Dielectric and polarization behavior of forsterite at elevated temperatures

RANDALL T. CYGAN,[1] ANTONIO C. LASAGA[2]

Department of Geosciences, Pennsylvania State University,
University Park, Pennsylvania 16802

ABSTRACT

The determination of the dielectric and polarization behavior of silicate minerals is important in the understanding of chemical bonding and the evaluation of interionic potentials in model calculations. The analysis of crystal-defect energetics and the atomistic theory of diffusion processes rely heavily upon the polarizability of component ions in the silicate. In this effort, dielectric constant (relative dielectric permittivity) and dielectric loss data have been obtained from capacitance measurements of single crystals of synthetic forsterite (Mg_2SiO_4) for orientations parallel to the **a**, **b**, and **c** crystallographic axes. Measurements were obtained as a function of temperature (25°C, 40–1000°C) and electric-field frequency (20 kHz–1 MHz). The static polarizabilities of forsterite at these temperatures are derived from the dielectric constants by utilizing the Clausius-Mosotti relation. The use of the polarizability additivity rule is confirmed for predicting the polarization of forsterite from the component oxides at high temperatures. Dielectric conductivities are determined from the dielectric loss values at 400–900°C and are in agreement with previous studies of single-crystal forsterite.

INTRODUCTION

In recent years there has developed an interest in quantifying the kinetics of geochemical and mineralogical processes. The comprehension of reaction mechanisms and of the approach of a mineral assemblage to equilibrium is vital for the application of geothermometry and geochronology, as well as for the analysis of mineral alteration, order-disorder status in minerals, crystal-growth and nucleation processes, and others. A useful and powerful technique in such an effort is the theoretical analysis of the basic atomic structure and energetics of the phases of concern. Although application of solid-state physics to ionic solids and other simple compounds has generally been met with success (see Kittel, 1976), there are limitations in analyzing the more complex atomistic nature of silicate minerals. The major hindrance in such an effort is evaluating the degree of covalency associated with the silicate mineral bonding, in particular the Si–O bond (Pauling, 1980), and the related polarization properties of the crystal (Lasaga and Cygan, 1982; Cygan and Lasaga, in prep.).

The recognition of the influential role of polarization in crystal bonding and lattice energies lies in the classic work of Mott and Littleton (1938). They determined the theoretical polarization energy about a lattice point that contains an excess of charge (i.e., a point defect) and ap-

plied it with success in evaluating the activation energy for ionic conduction in NaCl. This theory was extended by Lasaga (1980) in deriving formation energies of point defects in a silicate mineral, forsterite (Mg_2SiO_4). The anisotropic behavior of chemical diffusion in the orthorhombic forsterite was rationalized in the latter study.

The understanding of polarization phenomena in silicate minerals is of importance in numerous other geochemical applications. The incorporation of a polarizability term is necessary in the refinements of crystallattice energetics and dynamics (e.g., Iishi, 1978a, 1978b; Iishi et al., 1983; Cygan and Lasaga, in prep.), the calculation of point-defect formation and migration energies (Lasaga, 1980; Parker, 1983), and the evaluation of relaxation processes involving defect pairs. It is also possible in some cases to examine the type of defect structure a crystal possesses by an analysis of the dielectric polarization (Tilley, 1977). The role of polarization theory is therefore fundamental in the atomistic description of geochemical processes such as reaction kinetics, chemical diffusion, and the interpretation of intrinsic oxygen fugacities. There is an important need for the complete characterization of polarization effects in silicate minerals at geologically important temperatures.

The dielectric constant will define the polarization response for a material and can be measured as a function of frequency, temperature, applied field, pressure, oxygen fugacity, water content, crystallographic orientation, and composition. In silicate mineral studies, most electrical measurements have concentrated on the electrical conduction of olivines at upper-mantle conditions, usually in excess of 700°C and 700 MPa (7 kbar) (e.g., Bradley et

al., 1964; Shankland, 1969; Duba, 1972; Duba and Nicholls, 1973; Duba et al., 1974). These studies all examined laboratory samples at low frequencies (direct current to 1 kHz), corresponding to the situation in most geophysical field investigations such as geomagnetic and magnetotelluric surveys. Shankland (1975, 1981) and Duba (1976) provided reviews of the low-frequency conductivity measurements of the major rock-forming silicates, mantle-derived rocks, and their melt phases. For the present study, though, it is necessary to examine the electrical properties of minerals at high frequencies (greater than 1 kHz) in order to obtain the dielectric response that is void of major conduction and induction interferences. Olhoeft (1976) summarized the high-frequency measurement technique and the available dielectric behavior of selected minerals and rocks. Compilations of dielectric constants which include those for silicate minerals are given by Keller (1966), Westphal and Sils (1972), Young and Frederikse (1973), and Olhoeft (1981). Almost all of these data are for room-temperature measurements and polycrystalline samples (see Lasaga and Cygan, 1982).

In the present paper we present dielectric and polarizability data for a synthetic single crystal of forsterite at temperatures of 25°C and from 40 to 1000°C. There have been no previous dielectric studies of forsterite single crystals nor of polycrystalline forsterite at elevated temperatures. The basic theory is reviewed in the first section followed by a discussion of the experimental and measurement procedure. The results of the dielectric measurements of forsterite are then presented along with the derived high-frequency conductivity values. In the final section, we discuss the results in view of the forsterite crystal structure and transport properties.

BASIC THEORY

The fundamental relations necessary in our discussion of polarization in forsterite are provided in Lasaga and Cygan (1982). These basic electrical relationships are derived from the solutions to Maxwell's equations for electromagnetism. An excellent review of these electrical principles can be found in Jackson (1962). For the present discussion we will only be concerned with the basic equations required in evaluating the dielectric response of a material as measured in the laboratory. Von Hippel (1954) has provided a detailed review of dielectric theory and discussed numerous applications.

Although we require the static dielectric constant (i.e., at zero frequency) in the theoretical calculations, we are limited in the laboratory by additional polarization processes that prevent the measurement of the sample capacitance at direct current or low-frequency conditions. The capacitance is the basic measurable quantity, measured in farads (F) (= coulomb per volt), that determines the amount of charge a substance is able to store for a given electrical potential and is related by sample geometry to the dielectric constant. It is necessary to examine the frequency response of a material to an alternating electric field and sort out the contributing polarization factor (see Lasaga and Cygan, 1982).

An alternating electric potential source will produce a charging current, I_c, in a vacuum dielectric,

$$I_c = \frac{dq}{dt} = i\omega C_0 V, \tag{1}$$

where ω is the angular frequency of the electric field ($\omega = 2\pi\nu$; ν is the frequency in cycles per second or hertz), C_0 is the vacuum capacitance of the electrode configuration, V is the voltage at time t, and q is the charge ($q = C_0 V$). The imaginary value i ($\sqrt{-1}$) is required to describe the sine wave nature of the potential source as an exponential function [i.e., $\exp(i\omega t)$]. By incorporating a material sample (e.g., silicate mineral) between the measuring electrodes, the capacitance of the configuration will be increased:

$$C = C_0 \frac{\epsilon'}{\epsilon_0} = C_0 \kappa'. \tag{2}$$

Here, ϵ' and ϵ_0 denote the real dielectric constants (or permittivities) of the material and vacuum, respectively. The ratio of these values, κ', is referred to as the relative dielectric constant. The permittivity constant, ϵ_0, is a physical constant and has the value of 8.854×10^{-12} F/m. For the case of an ideal dielectric, the charging current will be 90° out of phase with the applied voltage.

There is an additional current, I_1, that is produced simultaneously with the charging current. The loss current is denoted by,

$$I_1 = GV, \tag{3}$$

where G is the conductance of the dielectric material and is usually expressed in units of siemens (S) where a siemens is defined as a reciprocal ohm (= farad per second). The total current for the dielectric material would then be given by

$$I = I_c + I_1 = (i\omega C + G)V. \tag{4}$$

Additionally, a loss angle δ defines the phase characteristics of this total current with respect to the charging current. In a real sample there are additional processes that contribute to the loss current besides the migration of charged species. Resistance heating of the sample, surface-electrode polarization, reorientation of associated atoms and point defects (i.e., dipoles), or any other energy-consuming process will create a dielectric loss response. Therefore, it is customary to include all of these loss processes and the charging dielectric behavior in a *complex* dielectric constant (see von Hippel, 1954):

$$\epsilon^* = \epsilon' - i\epsilon''. \tag{5}$$

The total current, Equation 4, can now be rewritten using Equations 2 and 5 as

$$I = (i\omega\epsilon' + \omega\epsilon'') \frac{C_0 V}{\epsilon_0}. \tag{6}$$

Here, the G conductance term has been incorporated in the imaginary part of the dielectric constant. Finally, a complex *relative* dielectric constant can be defined using terms analogous to those in Equation 5,

$$\kappa^* \equiv \frac{\epsilon^*}{\epsilon_0} = \kappa' - i\kappa'', \tag{7}$$

which gives the total current as

$$I = i\omega C_0 \kappa^* V. \tag{8}$$

The dielectric loss is usually measured in terms of the loss angle and is related to the ratio of complex to real components of the dielectric terms:

$$\tan\delta = \frac{\epsilon''}{\epsilon'} = \frac{\kappa''}{\kappa'}. \tag{9}$$

This term is often referred to as the dissipation factor (D) or the tangent loss. If a parallel RC circuit [i.e., a parallel resistor and

Table 1.   Mean chemical composition of synthetic forsterite determined by electron-microprobe analyses

| Oxide	Weight Percent	Standard Error	Cations/4 Oxygen
SiO$_2$	42.75	0.61	1.002
TiO$_2$	0.04	0.02	0.007
MnO	0.13	0.01	0.003
MgO	57.02	0.49	1.992
Total	99.94		3.004

Fig. 1.   Schematic drawing of the experimental setup denoting the four-terminal pair assembly. H and L refer, respectively, to the high and low leads of the current or potential connections.

capacitor where R is the resistance of the circuit (= $1/G$)] is utilized for modeling the sample in the measurement circuit, one would expect that

$$\tan \delta = \frac{I_l}{I_c} = \frac{1}{\omega RC}. \tag{10}$$

Any deviation of the dielectric loss from this behavior would suggest more than just a simple conductive loss current.

The real component of the relative dielectric constant of a sample can be evaluated by a measurement of the sample capacitance and knowledge of the geometry of the electrodes. For a parallel plate capacitor of area A and electrode separation d, the vacuum capacitance is given by

$$C_0 = \frac{A\epsilon_0}{d}. \tag{11}$$

Combining this expression with Equation 2 produces the following simple relationship for the real dielectric constant:

$$\kappa' = \frac{Cd}{\epsilon_0 A}. \tag{12}$$

It is assumed that any electric-field fringing effects about the sample edges are negligible.

The conductivity (σ) of a sample (often referred to as the specific conductance) is derived from Equations 2, 4, and 6 and is given by

$$\sigma = \omega\epsilon''. \tag{13}$$

An evaluation of the ϵ'' term can be obtained from a measurement of the dielectric loss. Therefore, this expression can be rewritten using Equations 2 and 9 to give

$$\sigma = \omega\epsilon_0\kappa' \tan \delta. \tag{14}$$

Conductivity is normally expressed in units of siemens per meter. The dielectric conductivity includes the contributions associated with energy-loss processes as well as those of the transport of charge carriers.

Several remarks are warranted at this time concerning the dielectric nomenclature and symbol usage. Major problems occur with the use of the term *relative* to define a dielectric constant and with the corresponding usage of κ or ϵ. The relative dielectric constant is denoted by κ and is dimensionless, whereas the dielectric constant ϵ has units of farad per meter. The latter term can always be compared to ϵ_0 in order to obtain the former (see Eq. 2). Theoretical treatments that require dielectric data refer to the *relative* dielectric value but traditionally denote it by the symbol ϵ. We have chosen this latter approach in Lasaga and Cygan (1982) and Cygan and Lasaga (in prep.) and will maintain such a position throughout the remainder of this paper. Therefore the real component of the relative dielectric constant will be
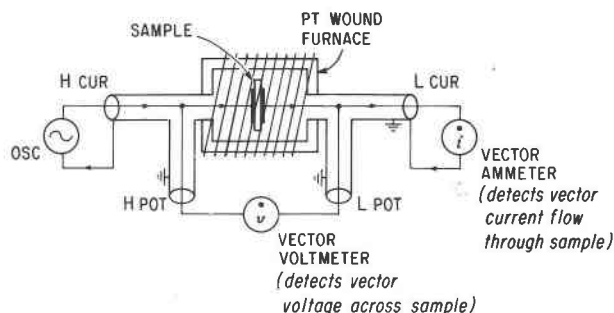
denoted by ϵ and will be treated as a dimensionless quantity. It should be noted, however, that the term dielectric *permittivity* has often been interchanged with dielectric *constant*, as the latter is seldom a true constant.

EXPERIMENTAL PROCEDURE

Single-crystal forsterite samples were obtained from synthetic oriented α-Mg$_2$SiO$_4$ boules that were originally produced by the Union Carbide Corporation. An average composition of the forsterite crystals obtained by electron-microprobe chemical analysis is presented in Table 1. The virtually pure Mg$_2$SiO$_4$ crystals proved to be homogeneous in composition. Disc-shaped samples were cut from each boule to provide orientations normal to the three crystallographic axes. Crystal orientations were verified to within 3° by use of the Laue back-reflection X-ray technique. Samples were ground with SiC powders to produce parallel plane faces and then polished down to 3 μm with γ-alumina. All samples were optically examined in reflected and transmitted light and were found to be free of fractures and inclusions. The sample discs were approximately 8 mm in diameter and 0.5 mm in thickness. Exact thicknesses were determined with a high-precision micrometer. All samples were ultrasonically cleaned in, successively, acetone, soapy water, distilled water, and ethanol and then dried in air at 110°C for 2 h.

The faces of each sample disc were coated with a Pt ink suspension to provide a conducting electrode surface. Two thin coats were applied with the samples being annealed in air at 1050°C for 12 h after each coating. Proper electrical conduction over the entire surface of each sample face was checked with an ohmmeter. The possibility of an electrical short across the edge of each sample was also checked and if present was corrected. An electrical short of even minor extent would provide a bypass of the forsterite sample and produce a false measurement of the dielectric properties. The area and circumference of the Pt electrodes were determined by projecting an image of the sample disc and digitizing the image with a GTCO Micro Datatizer system.

Room-temperature measurements were performed using a high-frequency capacitance bridge (Hewlett-Packard 4275A multi-frequency LCR meter) with the sample positioned in a plastic and Pt holder. For the high-temperature (40–1000°C) measurements, a completely automated setup was utilized with the 4275A LCR meter as the primary measuring unit. The meter is hooked up to a ceramic furnace assembly that is housed in the core of a 1-atm Pt-wound resistance furnace. Within this assembly, the samples are placed between two Pt foil squares that are in turn attached to Pt electrical leads. A spring-loaded support provides sufficient contact between the sample electrodes and the Pt foil. A four-

terminal pair connection is required in this setup to reduce any induced or stray capacitance. The entire ceramic assembly is coated with Pt paint and connected to a ground. The four-terminal pair leads are attached to the LCR meter via coaxial cables. A schematic representation of the experimental setup and measurement connections is presented in Figure 1.

The LCR meter is interfaced with a Hewlett-Packard 9825 computer which allows for the automatic reading and storage of capacitance and dielectric loss values. Temperatures are automatically recorded with a chromel-alumel thermocouple situated immediately next to the sample post. Temperature readings are believed to be accurate to within ±5°C. An interfaced power source and a separate thermocouple control the furnace heating rate during a run. A heating rate of 5°C/min proved to be satisfactory in obtaining thermal equilibrium for the particular sample size. A slower rate of 3°C/min was utilized for a single run as a check and produced equivalent capacitance readings. There was no detectable thermal hysteresis effect for the capacitance and loss measurements. As runs consisted of only a controlled heating cycle, it was only possible to examine this effect during a conductive cooling stage.

A high-temperature run was initiated by calibrating the LCR meter for open and short circuits. This process would remove any additional stray or induced capacitance leaks that could occur throughout the entire measurement circuit (i.e., LCR meter, cables, and sample assembly). It is important to remove all possible interfering capacitance from the measurement circuitry owing to the extremely low capacitances of the forsterite samples [on the order of 5–20 pF (picofarad = 10^{-12} F)]. The forsterite values are close to the minimum detection level of the LCR meter. Because of the restriction imposed by the single-crystal geometries, it was not possible to increase the measured capacitance by major changes in the sample thickness and electrode area (see Eq. 12).

Measurements of capacitance and dielectric loss were performed at each of the following high-frequency values: 20, 40, 100, and 400 kHz and 1 MHz. The accuracy of these measurements varies with frequency and is discussed in Hewlett-Packard (1979). The actual measurement error will be a combination of these specification errors and those associated with the electrode configuration of the sample assembly. A worst-case estimate of the uncertainty in measured capacitance provides the following values: at 20 kHz, 0.02 pF; at 40 kHz, 0.07 pF; at 100 kHz, 0.06 pF; at 400 kHz, 0.03 pF; and at 1 MHz, 0.02 pf. The relative error in the loss measurements is estimated to be 5% for all frequencies. These errors are considerably greater than those presented in the LCR meter operating manual (Hewlett-Packard, 1979). The room-temperature measurements provided a greater range in frequencies (10 kHz–10 MHz). The four-terminal pair electrode method provides a measurement of the vector voltage across the sample electrodes and the vector current flow through the sample. The imaginary component of these two vector quantities provides the capacitance value, and the real component provides the dielectric loss value (see Eq. 4). The LCR meter was maintained in parallel RC mode as would be appropriate for an equivalent circuit model of the electric behavior of the forsterite samples. The test-signal voltage level was kept at a value of 1.00 V. Measurements were taken at each of the frequencies for every 5°C interval from 40°C to 1000°C. It was necessary to momentarily cut power to the furnace during the measurements for a given temperature in order to prevent any induced capacitance from the current flow of the Pt windings.

In order to completely define the dielectric properties of forsterite, it was necessary to obtain dielectric data for the three crystallographic axes. Forsterite, as an orthorhombic silicate, possesses dielectric anisotropy that can be expressed by the diagonal terms of the dielectric tensor (Nye, 1957; Cygan and Lasaga, in prep.). Because of the limited availability of the forsterite single-crystal boules, we were only able to obtain a duplicate sample for the c crystallographic direction. All samples were remeasured several times at 25°C and at high temperatures and provide results in agreement within the experimental uncertainties. It was necessary to repeat the sample and Pt-electrode preparation for the additional runs.

All measured capacitance values were corrected for electric-field edge effects using the ASTM (1981) recommended scheme. The correction, a function of sample thickness and electrode circumference, reduces the measured capacitance by no more than 5%. Thermal-expansion corrections were also required to provide the correct sample dimensions at the measured temperature. Linear-expansion coefficients were derived from the high-temperature crystal-structure data of Hazen (1976) and were incorporated to account for the increased sample thickness and the larger electrode area. The dielectric constants were obtained directly from Equation 12 using the corrected capacitance and sample-geometry values. The thermal corrections are minor and account for less than 2% of the dielectric constant. The standard errors associated with the dielectric constant determination were derived by conventional error-propagation techniques based upon the measurement uncertainties in capacitance and sample geometry. The relative uncertainties of the dielectric constants are on the order of 1.5–4.0%, being predominated by the uncertainty in the sample thickness measurement.

The dielectric conductivities for each sample were evaluated by using Equation 14 and the dielectric data obtained at 20 kHz and in the temperature range of 400–900°C. Conductivities were not evaluated beyond both temperature extremes owing to either loss interferences at high T (see below) or loss values below the detection limit at low T. The larger loss values obtained at the 20-kHz frequency were utilized in order to improve the accuracy of the measurement. It was assumed that these conductivities are independent of frequency (see Bradley et al., 1964; Duba, 1972) and that a comparison can be made directly with those obtained at low frequencies (less than 1 kHz) (A. Duba, Lawrence Livermore National Laboratory, pers. comm.). Of course, there may exist additional mechanisms besides charge-carrier migration that contribute to the dielectric loss and, therefore, to the calculated dielectric conductivity. The relative standard error for the conductivity values is estimated to be approximately 5%.

RESULTS

The results of the room-temperature determination of the forsterite relative dielectric constants are presented in Table 2. Also included are the static polarizabilities, α, derived from the dielectric values using the Clausius-Mosotti relation (see Lasaga and Cygan, 1982):

$$\alpha = \frac{3V}{4\pi} \frac{\epsilon - 1}{\epsilon + 2}. \tag{15}$$

Here, V is now the molecular volume of a Mg_2SiO_4 unit (72.45 Å³), and ϵ refers to the real component of the relative dielectric constant. The uncertainties in α were obtained by a propagation-of-error method. The dielectric constants were obtained at 1 MHz and are free from the interferences of extraneous polarization processes (see below). These values represent the static dielectric constant

Table 2. Dielectric constants and corresponding polarizabilities for synthetic forsterite measured at 1 MHz and 25°C (uncertainties represent one standard deviation)

Crystallographic Orientation	ϵ Dielectric Constant	α Polarizability (A^3)
a (100)	6.97 ± 0.21	11.51 ± 0.14
b (010)	7.71 ± 0.24	11.95 ± 0.14
c (001)	7.11 ± 0.21	11.60 ± 0.13

and include only the contribution of ionic and electronic polarization (Lasaga and Cygan, 1982).

Figure 2 provides a plot demonstrating the dependence of the forsterite dielectric constant upon frequency (i.e., $\log \nu$). Data are presented for the **b** axis orientation at room temperature (25°C) and at selected high temperatures; similar results were obtained for the forsterite **a** and **c** axes. The data at 25°C illustrate the change in forsterite polarization processes that one expects in going from a relatively low frequency or static region (ionic plus electronic polarization) to the high-energy optical frequencies (electronic-only polarization). In the optical region the dielectric constant is given as the square of the refractive index. The transition between the two polarization processes, schematically drawn in Figure 2, is referred to as the infrared-dispersion region. On a theoretical basis one would expect the dielectric constant to approach positive and negative infinity values through this transition.

For the higher temperatures the polarization contributions of space charge, interfacial effects, crystal inhomogeneity, and crystal defects are apparent by the increase of the dielectric constant in the lower-energy range of the measured frequencies (below 100 kHz). The forsterite
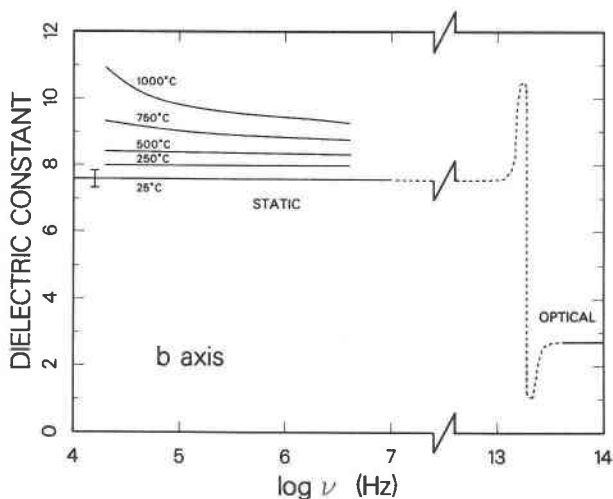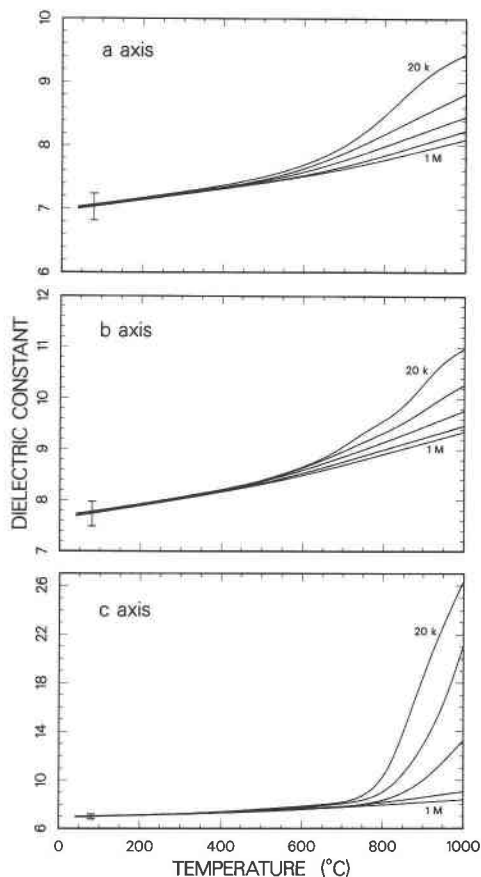

Fig. 3. Dielectric constant for the three crystallographic orientations of forsterite obtained at selected frequencies (20, 40, 100, and 400 kHz and 1 MHz) as a function of temperature. Frequency labels are in units of hertz. Error bar represents the measurement uncertainty in the dielectric constant.

Fig. 2. Dielectric constant for the **b**-axis orientation of forsterite determined at selected temperatures as a function of the logarithm of the electric-field frequency. Error bar denotes measurement uncertainty in the dielectric constant.

sample produces a greater dielectric response owing to the distortion of the macroscopic electric field created by these polarizations. The large increase in dielectric constant is also partly explained by a corresponding increase of the defect concentrations intrinsically produced with temperature. All of the dielectric constant curves tend to flatten out at the 1-MHz frequency from which static dielectric values are used to calculate the polarizability.

Figure 3 presents the temperature dependence of the dielectric constant of forsterite parallel to the **a**, **b**, and **c** crystallographic axes. Separate curves are given for each of the measured frequencies. Similarly, the dielectric loss values corresponding to these dielectric constant measurements are provided in Figure 4. Loss values greater than unity have been removed from the lower-frequency curves to provide detail of the higher-frequency loss measurements. All three crystallographic orientations exhibit an initial linear increase of the dielectric constant with temperature followed by a break in slope at approximately 500°C and then an increasing change up to 1000°C. The break in slope is represented in the dielectric loss data and indicates the transition of forsterite from an insulator to
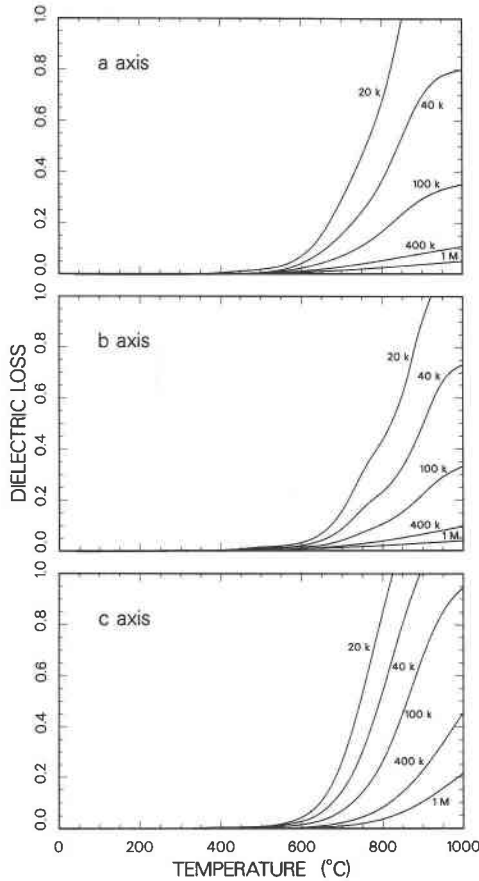
Fig. 4. Dielectric loss for the three crystallographic orientations of forsterite measured at selected frequencies as a function of temperature. Frequency labels are in units of hertz. The loss data have a relative uncertainty of approximately 5%.
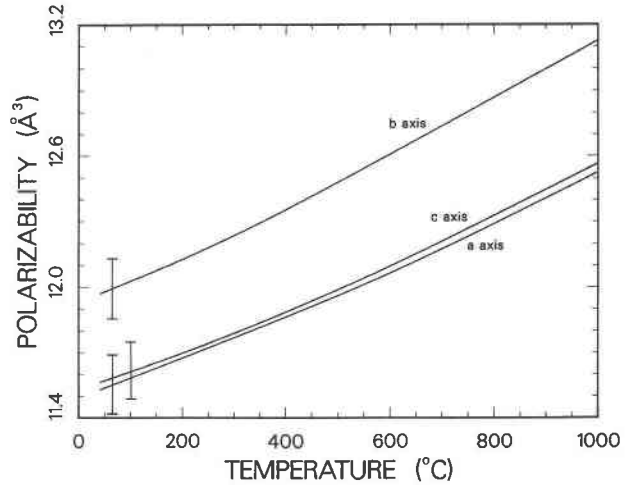

Fig. 5. Static polarizabilities for the three crystallographic directions of forsterite as a function of temperature. Error bars denote the standard uncertainty associated with the calculated polarizability.

E_a represents the activation energy for conduction, σ_0 is the usual preexponential term, R is the gas constant, and T is the absolute temperature. Conductivity values were determined only at the temperatures where Equation 10 was satisfied. A plot of log tan δ versus log ω provided a slope of approximately negative unity and suggested the existence of a simple conduction mechanism in this temperature range. The activation energies and σ_0 terms, derived from Equation 16, are provided in Table 4. Figure 6 presents an Arrhenius plot (log σ versus $1/T$) of the results obtained for each crystallographic orientation. Also included in Figure 6 are the low-frequency (less than 1 kHz) conductivities measured for pure forsterite obtained from previous studies.

DISCUSSION

The dielectric data presented in the previous section provide the necessary parameters for evaluating the polarization behavior of forsterite at realistic geologic temperatures. A salient point of these data is the existence of a dielectric anisotropy that will affect the directional characteristics of transport properties (e.g., chemical diffusion and conduction). The 1-MHz frequency data indicate that for all temperatures the relative values of the dielectric constants of the three orthogonal orientations are

a conductor. The minor fluctuations in the dielectric constant and loss curves can be attributed to the measurement sensitivity and the influence of low-intensity polarization effects such as the interruption of charge migration and electrode-sample interference (see discussion).

Static polarizabilities were derived from the ϵ (1 MHz) versus T data using the Clausius-Mosotti relation (Eq. 15) and are presented in Figure 5. The dependence of Mg_2SiO_4 volume upon temperature was taken from the olivine-structure data of Hazen (1977). The higher-temperature polarizabilities (greater than 600°C) required the extrapolation of the low-temperature dielectric constant data in order to subtract out the high-temperature interferences.

The first-order temperature derivatives of the static dielectric constant and polarizability for each forsterite orientation are listed in Table 3. These terms were evaluated for the dielectric data measured at 1 MHz and 40–600°C.

The dielectric conductivities of forsterite at 400–900°C were derived from Equation 14 and were fitted to the following Arrhenius equation expected of a thermally activated process:

$$\sigma = \sigma_0 \exp\left(-\frac{E_a}{RT}\right). \qquad (16)$$

Table 3. Temperature derivatives of the static (1 MHz) dielectric constant and polarizability for forsterite (uncertainties represent one standard deviation)

Crystallographic Orientation	$\frac{1}{\epsilon}\left(\frac{\partial \epsilon}{\partial T}\right)_p \times 10^4$ (/K)	$\frac{1}{\alpha}\left(\frac{\partial \alpha}{\partial T}\right)_p \times 10^4$ (/K)
a (100)	1.22 ± 0.14	0.79 ± 0.06
b (010)	1.69 ± 0.12	0.90 ± 0.08
c (001)	1.24 ± 0.20	0.78 ± 0.12

Table 4. Arrhenius parameters for describing the dielectric conductivity of forsterite for 400–900°C (uncertainty in E_a represents the standard deviation derived from the linear regression)

Crystallographic Orientation	σ_0 (S/m)	E_a (kJ/mole)
a (100)	0.10	87 ± 6
b (010)	0.17	94 ± 8
c (001)	1.20	106 ± 7

$\epsilon_b > \epsilon_c \simeq \epsilon_a$. It is not possible to distinguish between the a- and c-axis values because of the experimental uncertainties. The static polarizabilities will necessarily demonstrate the same relative anisotropy (see Fig. 5). The optical dielectric constants of forsterite, derived from the refractive index data of Kerr (1977), indicate a reversal of relative values: $\epsilon_a^{opt} > \epsilon_c^{opt} > \epsilon_b^{opt}$. These data suggest the occurrence of a crossover in the infrared transition zone for the relative dielectric anisotropy.

Lasaga and Cygan (1982) discussed the importance of incorporating the polarization energy in the defect-formation calculations for forsterite (see Lasaga, 1980). Relaxation of the crystal lattice through polarization effects would also be important in the migration of ions in forsterite. Therefore, chemical diffusion of ions would be sensitive to the dielectric anisotropy of forsterite. The oxygen-diffusion studies of Reddy et al. (1980) and Jaoul et al. (1983) for forsterite report a preferred transport of oxygen along the b crystallographic direction while the a and c directions provided slower diffusion rates ($D_b > D_a \geq D_c$). These observations are in agreement with the observed dielectric anisotropy. One would expect preferred mobility along the greatest polarization direction owing to the relative ease of creating and migrating a point defect or ion. For the case of forsterite, the bulk of the polarizability is attributed to the oxygen anion, based on the additivity rule for ionic constituents (see Lasaga and Cygan, 1982). This also follows from the much larger ionic size of oxygen relative to the cations creating a larger deformation or polarization character. It is only possible to compare the diffusion data for oxygen to the measured polarizabilities and dielectric constants.

As mentioned previously, the ϵ versus T curves deviate from a linear behavior at higher temperatures. Certain fluctuations can be correlated to those in the dielectric loss curves. Although these anomalies are within the measurement uncertainty, they suggest the occurrence of additional polarization and loss processes and therefore the breakdown of the simple parallel RC equivalent circuit used to measure the dielectric response. Because of the extremely low sample capacitance being measured, minor contributions will be reflected in the curvature of the temperature plots, especially for the low frequencies. Breckenridge (1952) and Economou (1964) suggested that such anomalous behavior for the dielectric loss of simple ionic crystals can be attributed to a relaxation process involving dipoles (e.g., impurity or vacancy-defect pairs), whereas
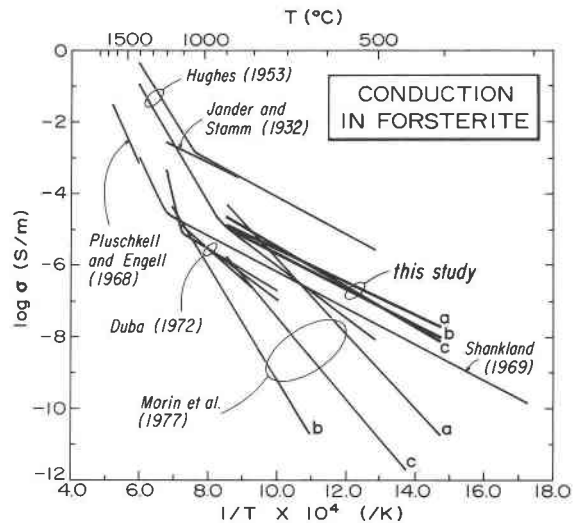

Fig. 6. Arrhenius plot demonstrating the variation of forsterite conductivity with temperature. The heavy solid lines denote the dielectric conductivities measured in this study for the three crystallographic directions of Mg_2SiO_4.

Bielig and Lilley (1980) indicated charged dislocation lines to be the major mechanism. We were unable to reproduce the dielectric loss anomalies for replicate runs with forsterite and therefore suggest a sample preparation problem, possibly an unsuitable sample surface and improper contact with the Pt electrodes. Another factor may be the interruption of charge migration by the trapping of charge carriers such as electrons, electron holes, ions, or vacancies in the sample or at the electrode interface. If vacancy pairs did exist in large concentrations in forsterite, one would expect a reorientation of the vacancy-pair dipole with the alternating electric field and would observe an anomalous dielectric loss when the measurement frequency is equivalent to the appropriate reorientation frequency. Such dielectric responses as a function of temperature would provide formational enthalpies for the defect pair. However, limitations are imposed on our measurements by the low capacitance values for forsterite and the level of accuracy of the present-day capacitance bridges.

With the available high-temperature polarizabilities of forsterite it is possible to examine the feasibility of the additivity rule. Lasaga and Cygan (1982) presented a scheme for predicting the total polarizability of a silicate by the summation of the individual oxide polarizabilities. Although we are restricted by the paucity of dielectric data for silicates and relevant oxides at elevated temperatures, it is possible to examine forsterite at 500°C. Using the dielectric constants of MgO and SiO_2 measured at 500°C (Westphal and Sils, 1972), we calculated polarizabilities of, respectively, 3.45 Å³ and 5.82 Å³, which predict a forsterite static polarizability of 12.72 Å³ (see Eq. 10 of Lasaga and Cygan, 1982). The high-temperature measurements on forsterite suggest a polarizability of 12.21 Å³ based on an averaging of the dielectric constant anisotropy. These values are in approximate agreement; the additivity rule overestimates the measured value by 4%.

For room-temperature data, the oxide-additivity rule predicts a forsterite polarizability of 11.48 Å³ compared to the measured value of 11.74 Å³ (2% difference). It appears that at higher and more geologically interesting temperatures, the polarizability for a given silicate mineral can be approximated by an additivity rule. Until more refined high-temperature dielectric measurements are performed on other important rock-forming silicates, it will be necessary to utilize the additivity rule for mineralogical model calculations.

Knowledge of the temperature derivative of the polarizability for forsterite is important if we are to generalize and extend its application to other similar-structure silicates (e.g., garnet) for which high-temperature data are lacking. The straightforward increase of polarizability with temperature is apparent in Figure 5. The average of the numerically evaluated temperature derivatives for ϵ and α is presented in Table 3 for each forsterite orientation. The relative change in α with temperature at constant pressure can be described by differentiating Equation 15:

$$\frac{1}{\alpha}\left(\frac{\partial\alpha}{\partial T}\right)_P = \frac{3}{(\epsilon-1)(\epsilon+2)}\left(\frac{\partial\epsilon}{\partial T}\right)_P + \frac{1}{V}\left(\frac{\partial V}{\partial T}\right)_P. \quad (17)$$

The two contributing factors in Equation 17 are the temperature dependence of the dielectric constant and the thermal expansion coefficient. The increase of polarizability with temperature is expected on fundamental grounds. At higher temperatures, the mean bond distances are greater and the force constants between ions are therefore lower. This enables the ionic polarization to increase. The electronic contribution to the total polarization is expected to be independent of temperature. The α versus T behavior is significant in that it reflects ionic interactions and can be used to constrain interionic potentials for silicate minerals (see Cygan and Lasaga, in prep.).

The dielectric conductivities presented in Figure 6 are noteworthy in that there appears to be little anisotropy exhibited for the temperature range of 400–900°C. At the lower temperatures we observe that $\sigma_a > \sigma_b \simeq \sigma_c$, whereas at temperatures above 650°C $\sigma_c > \sigma_b \simeq \sigma_a$. The relative values of the higher-temperature conductivity data agree with the measured cation-diffusion anisotropy reported by Buening and Buseck (1973). The minor anisotropic behavior of the conductivities is in marked disagreement with the only other conductivity study of oriented single-crystal forsterite; polycrystalline and nonoriented samples have generally been measured. Morin et al. (1977) observed major anisotropic behavior, up to four orders of magnitude, based on DC measurements during cooling of the samples. The activation energies for conduction in forsterite based upon our measurements (see Table 4) are in good agreement with those derived for nonoriented single-crystal samples (e.g., Shankland, 1969; Duba, 1972). Although conductivities by themselves are insufficient for determining the actual conduction mechanism, most studies attribute these activation values to an extrinsic ionic transport mechanism. The conductivity data at temperatures in excess of 1100°C suggest a different conduction mechanism as evidenced by the "kink" in the Arrhenius plot. These higher activation energies (on the order of 300 kJ/mol) suggest an intrinsic ionic migration and are comparable to the cation-diffusion energies obtained for olivines (see Buening and Buseck, 1973; Morioka, 1980, 1981). It is of significance to note that these diffusion studies provide Arrhenius plots that exhibit similar "kinks."

In an extrinsic process the defect structure of the crystal, and hence the transport properties, will be controlled by the concentration of impurities. For silicate minerals, in particular forsterite, a major impurity will be iron. Because of the multivalent nature of Fe, one would expect a major dependence of the conductivity upon oxygen fugacity as well as total Fe concentration. This f_{O_2} dependency has been verified for the case of conduction (e.g., Duba and Nicholls, 1973; Duba et al., 1974) and cation diffusion (e.g., Buening and Buseck, 1973) in olivines. The dielectric measurements of the present study were completed in static air, but no evidence of oxidation was noted upon optical examination of the sample edges after completion of the run. As a measure of conduction in forsterite, the dielectric loss would be most sensitive to oxygen fugacity and Fe^{3+}/Fe^{2+} changes. The dielectric constant (capacitance) measurements would be less affected, although no investigation has been carried out. Future studies would necessarily examine the role of major impurities and oxygen fugacity in contributing to the observed dielectric behavior of forsterite.

CONCLUSION

Early examinations of the dielectric properties of rocks and minerals were as a rule limited by problems involving impurities, water content, polycrystallinity, and measurement accuracy (e.g., Takubo et al., 1953a, 1953b; Keller and Licastro, 1959). High-temperature measurements were ignored owing to interests in utilizing dielectric properties as a prospecting and mineral survey technique. Recently, the use of theoretical models by mineralogists has developed a need for accurate dielectric constant values in order to investigate the nature of bonding in silicate phases. The high-temperature dielectric data of forsterite are an obvious improvement over the earlier studies and provide values useful at relevant temperatures for evaluating geochemical processes.

We feel that the present study has been successful in defining the polarization behavior of single-crystal forsterite as a function of temperature, frequency, and crystal orientation. These data can now be employed with confidence in point-defect and lattice-energy calculations. The verification of the polarizability additivity rule at geologically interesting temperatures also suggests the possibility of application to other rock-forming silicate minerals.

REFERENCES

ASTM. (1981) Standard test methods for A-C loss characteristics and permittivity (dielectric constant) of solid electrical insulating materials. In 1981 annual book of ASTM standards, ANSI/ASTM-D-150-80, Part 35, 49–72. American Society for Testing and Materials, Philadelphia.

Bielig, G.A., and Lilley, E. (1980) The dielectric loss of crystals of NaCl: Cd^{2+} following plastic deformation. Philosophical Magazine A, 41, 745–760.

Bradley, R.S., Jamil, A.K., and Munro, D.C. (1964) The electrical conductivity of olivine at high temperatures and pressures. Geochimica et Cosmochimica Acta, 28, 1669–1678.

Breckenridge, R.G. (1952) Relaxation effects in ionic crystals. In W. Shockley et al., Eds. Imperfections in nearly perfect crystals, 219–245. Wiley, New York.

Buening, D.K., and Buseck, P.R. (1973) Fe-Mg lattice diffusion in olivine. Journal of Geophysical Research, 78, 6852–6862.

Duba, Al. (1972) Electrical conductivity of olivine. Journal of Geophysical Research, 77, 2483–2495.

——— (1976) Are laboratory electrical conductivity data relevant to the earth? Acta Geodaetica, Geophysica et Montanistica, 11, 485–495.

Duba, Al, and Nicholls, I.A. (1973) The influence of oxidation state on the electrical conductivity of olivine. Earth and Planetary Science Letters, 18, 59–64.

Duba, Al, Heard, H.C., and Snock, R.N. (1974) Electrical conductivity of olivine at high pressure and under controlled oxygen fugacity. Journal of Geophysical Research, 79, 1667–1673.

Economou, N.A. (1964) Dielectric loss of potassium chloride. Physical Review, 135, A1020–A1022.

Hazen, R.M. (1976) Effects of temperature and pressure on the crystal structure of forsterite. American Mineralogist, 61, 1280–1293.

——— (1977) Effects of temperature and pressure on the crystal structure of ferromagnesian olivine. American Mineralogist, 62, 286–295.

Hewlett-Packard. (1979) Operating manual model 4275A multi-frequency LCR meter. Yokogawa-Hewlett-Packard, Tokyo.

Hughes, H. (1953) The electrical conductivity of the Earth's interior. Ph.D. thesis, University of Cambridge, Cambridge.

Iishi, Kazuaki. (1978a) Lattice dynamical study of the α-β quartz phase transition. American Mineralogist, 63, 1190–1197.

——— (1978b) Lattice dynamics of forsterite. American Mineralogist, 63, 1198–1208.

Iishi, Kazuaki, Miura, Mitiko, Shiro, Yuji, and Murata, Hiromu. (1983) Lattice dynamics of α-quartz including the effect of the width of the atomic electron distribution. Physics and Chemistry of Minerals, 9, 61–66.

Jackson, J.D. (1962) Classical electrodynamics. Wiley, New York.

Jander, W., and Stamm, W. (1932) Der innere Aufbau fester anorganischer Verbindungen bei hoheren Temperaturen. Zeitschrift für Anorganische und Allgemeine Chemie, 207, 289–307.

Jaoul, Olivier, Houlier, Bernard, and Abel, Francois. (1983) Study of ^{18}O diffusion in magnesium orthosilicate by nuclear microanalysis. Journal of Geophysical Research, 88B, 613–624.

Keller, G.V. (1966) Electrical properties of rocks and minerals. In S.P. Clark, Jr., Ed. Handbook of physical constants, 553–577. Geological Society of America Memoir 97.

Keller, G.V., and Licastro, P.H. (1959) Dielectric constant and electrical resistivity of natural-state cores. U.S. Geological Survey Bulletin 1052-H, 257–285.

Kerr, P.F. (1977) Optical mineralogy. McGraw-Hill, New York.

Kittel, Charles. (1976) Introduction to solid state physics. Wiley, New York.

Lasaga, A.C. (1980) Defect calculations in silicates: Olivine. American Mineralogist, 65, 1237–1248.

Lasaga, A.C., and Cygan, R.T. (1982) Electronic and ionic polarizabilities of silicate minerals. American Mineralogist, 67, 328–334.

Morin, F.J., Oliver, J.R., and Housley, R.M. (1977) Electrical properties of forsterite, Mg_2SiO_4. Physical Review B, 16, 4434–4445.

Morioka, Masana. (1980) Cation diffusion in olivine—I. Cobalt and magnesium. Geochimica et Cosmochimica Acta, 44, 759–762.

——— (1981) Cation diffusion in olivine—II. Ni-Mg, Mn-Mg, Mg and Ca. Geochimica et Cosmochimica Acta, 45, 1573–1580.

Mott, N.F., and Littleton, M.J. (1938) Conduction in polar crystals. I. Electrolytic conduction in solid salts. Faraday Society Transactions, 34, 485–499.

Nye, J.F. (1957) Physical properties of crystals. Clarendon Press, Oxford.

Olhoeft, G.R. (1976) Electrical properties of rocks. In R.G.J. Strens, Ed. The physics and chemistry of minerals and rocks, NATO Advanced Study Institute, 261–278. Wiley, London.

——— (1981) Electrical properties of rocks. In Y.S. Touloukian et al., Eds. Physical properties of rocks and minerals, 257–330. McGraw-Hill, New York.

Parker, S.C. (1983) Computer modelling of minerals. Ph.D. thesis, University College London, London.

Pauling, Linus. (1980) The nature of silicon-oxygen bonds. American Mineralogist, 65, 321–323.

Pluschkell, V.W., and Engell, H.J. (1968) Ionen und Elektronenleitung im Magnesium Orthosilikat. Berichte der Deutschen Keramischen Gesellschaft, 45, 388–394..

Reddy, K.P.R., Oh, S.M., Major, L.D., and Cooper, A.R. (1980) Oxygen diffusion in forsterite. Journal of Geophysical Research, 85, 322–326.

Shankland, T.J. (1969) Transport properties of olivines. In S.K. Runcorn, Ed. The application of modern physics to the earth and planetary interiors, NATO Advanced Study Institute, 175–190. Wiley, New York.

——— (1975) Electrical conduction in rocks and minerals: Parameters for interpretation. Physics of the Earth and Planetary Interiors, 10, 209–219.

——— (1981) Electrical conduction in mantle materials. In R.J. O'Connell and W.S. Fyfe, Eds. Evolution of the earth, American Geophysical Union Geodynamics Series, 5, 256–263.

Takubo, Jitsutaro, Ukai, Yasuo, and Kakitani, Satoru. (1953a) On the dielectric constants of minerals. Mineralogical Journal, 1, 3–24.

Takubo, Jitsutaro, Ukai, Yasuo, and Kuo, C.C. (1953b) On the dielectric constants of rocks. Mineralogical Journal, 1, 25–35.

Tilley, R.J.D. (1977) Correlation between dielectric constant and defect structure of non-stoichiometric solids. Nature, 269, 229–231.

von Hippel, A.R. (1954) Theory. In A.R. von Hippel, Ed. Dielectric minerals and applications, 3–46. Wiley, New York.

Westphal, W.B., and Sils, Aina. (1972) Dielectric constant and loss data. U.S. National Technical Information Service, AFML-TR-72-39.

Young, K.F., and Frederikse, H.P. (1973) Compilation of the static dielectric constants of inorganic solids. Journal of Physical and Chemical Reference Data, 2, 313–409.